Matter

CellPress

Article

Displacement vorticity as the origin of moiré potentials in twisted $WSe_2/MoSe_2$ bilayers

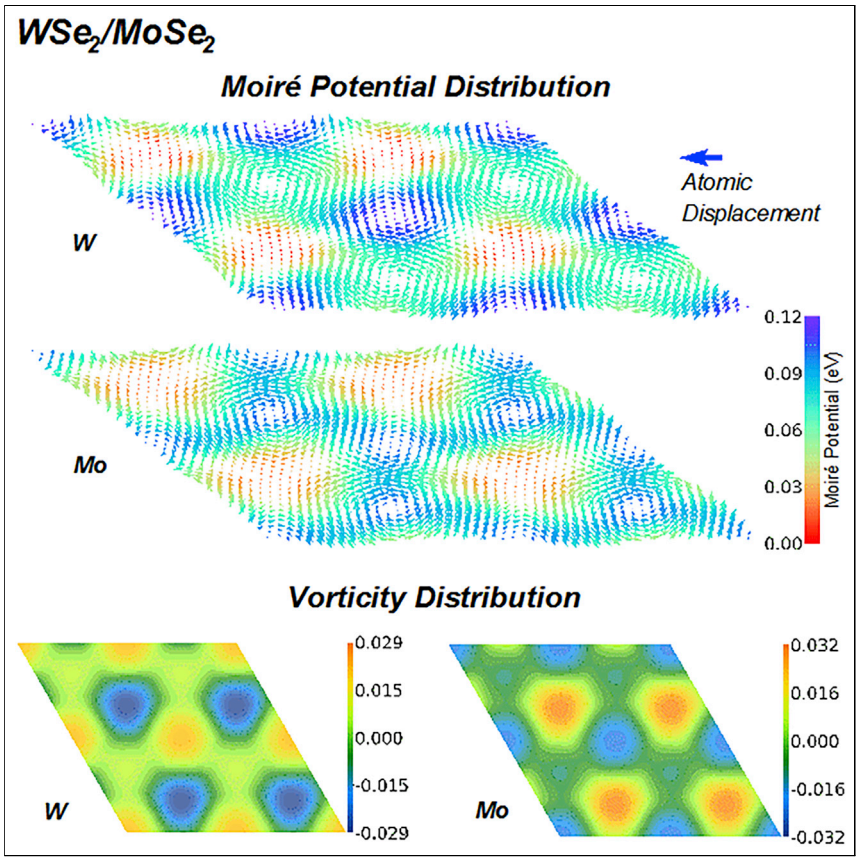

Geng et al. introduce the vorticity of atomic displacement into the deformation tensor in twisted van der Waals bilayers, where a moiré pattern of modulated interlayer coupling generates intralayer local lattice rotation. Their first-principles study reveals that it is mainly the displacement vorticity that determines the moiré potentials in slightly twisted $WSe_2/MoSe_2$ bilayers with marginal normal strain. Exploration of the vorticity tensor of local lattice rotation in solids could have profound impact in twistronics and condensed-matter physics in general.

Wen Tong Geng, Jian Bo Lin, Vei Wang, Qiang Gu, Qing Peng, Takahisa Ohno, Jun Nara

geng@hainanu.edu.cn (W.T.G.)
nara.jun@nims.go.jp (J.N.)

Highlights

Intralayer local lattice rotation can be significant in twisted van der Waals bilayers

Vorticity of atomic displacements is introduced to describe the lattice deformation

Displacement vorticity produces strong moiré potentials in $WSe_2/MoSe_2$ bilayers

1 **Discovery**
A new material or phenomena

Geng et al., Matter 6, 493–505
February 1, 2023
https://doi.org/10.1016/j.matt.2022.11.014

Matter

CellPress

Article

Displacement vorticity as the origin of moiré potentials in twisted $WSe_2/MoSe_2$ bilayers

Wen Tong Geng,[1,2,6,*] Jian Bo Lin,[2] Vei Wang,[3] Qiang Gu,[4] Qing Peng,[5] Takahisa Ohno,[2] and Jun Nara[2,*]

SUMMARY

The moiré potential induced by nonuniform interlayer coupling in a twisted van der Waals bilayer manifests itself in excitons, trions, and many other exotic electronic and optical properties, yet its origin remains elusive. Strains are generally believed to give rise to the moiré potential in a complicated way through lattice deformation. Our density functional theory calculations on twisted $WSe_2/MoSe_2$ heterobilayers ($2.5^\circ < \theta_M < 10^\circ$) confirm that lattice deformation plays a dominant role but reveal that the marginal normal strain makes only minor contributions, and that the shear strain is not correlated directly to the moiré potential. It is found that the vorticity of atomic displacements, that is, the local lattice rotation, rather than strains in the moiré cells, determines, to a large extent, the moiré potential. This discovery sheds new light on the understanding of the roles of distortion in twistronics and will be instructive in electronic structure engineering of moiré materials.

INTRODUCTION

There are a vast variety of novel quantum phenomena in condensed mater physics, such as such as Hofstadter's spectra,[1,2] moiré excitons,[3–6] Wigner crystal states,[7,8] and moiré trions[9] in nanoscale moiré patterns, that are formed by small lattice mismatch and/or twist angle in van der Waals (vdW) homo- or heterobilayers. Moiré physics, or twistronics,[10] has indeed emerged as one of the most rapidly developing research fields in semiconductor physics in the past decade since the pioneering work by Bistritzer and MacDonald.[11] Moiré potentials, the spatial change of the energy level of valence and conduction bands and of the band gap, are fundamental physical quantities of the interlayer coupling in a moiré pattern, the twist-angle dependence of which governs the optical properties of the bilayer superlattice. Precise determination of moiré potentials present challenges to both measurements and first-principles computational studies. The former require defect-free material and highly accurate control of the small twist angles, and the latter are extremely demanding in employing huge superlattices.[12,13]

In transition-metal dichalcogenide (TMDC) bilayer moiré cells larger than several nanometers, the three regions with 3-fold symmetry have local atomic structure very similar to the corresponding twist-free stackings, yet with a small twist angle. First-principles calculations of the ideal high-symmetry TMDC stackings showed that the variation of the valence band maximum (VBM) and conduction band minimum (CBM) among these twist-free TMDC bilayers is only of the order of 0.01 eV.[14] Recent experimental measurements by Shabani et al.[12] demonstrate that the moiré potentials in a $WSe_2/MoSe_2$ bilayer heterobilayer with a twist angle $\theta_M \approx 1.5^\circ$ can reach 0.3 eV for the VBM and 0.15 eV for the CBM. It is quite clear that

PROGRESS AND POTENTIAL

Bilayer moiré superlattices formed by stacking two van der Waals single layers with a small twist angle emerge as a prolific land to explore a wide range of novel electronic phases and devices. The moiré potentials modulating the interlayer interaction give rise to new condensed matter physics, and the understanding of their origin from lattice deformation is highly imperative in engineering moiré devices.

The deformation tensor in a condensed matter includes strain tensor as the symmetric part and vorticity tensor as the antisymmetric part. Unlike in fluid, external stress usually cannot generate vorticity tensor in solids. In twisted van der Waals bilayers, the vorticity tensor emerges due to moiré patterns. This study reveals that it is mainly the displacement vorticity that generates moiré potentials in $WSe_2/MoSe_2$ bilayers. Exploration of vorticity tensor in moiré systems could have profound impact in moiré physics, materials science, and nanotechnologies for 2D systems.

the lattice deformation resulting from nonuniform interlayer coupling, rather than direct interlayer coupling, is the dominant factor in determining moiré potentials. Nevertheless, we noticed that in Shabani et al.,[12] the shear strain calculated by continuum mechanics vanishes at the high-symmetry points, where the moiré potentials take their extreme values. The normal strain, on the other hand, is negligibly small throughout the moiré cell. This strongly indicates that shear strain does not influence the moiré potentials in a direct way, as was found in TMDC monolayers.[15–17]

Inspired by the fact that 2D membranes embedded in 3D space have a tendency to crumple[18] and the ease of rippling in graphene,[19] we propose to view a vdW monolayer as a fluid in a discussion of its lattice deformation. An essential part of fluid dynamics is vorticity,[20] which stands for the antisymmetric part of deformation tensor. Here, in a solid monolayer, the analog of vorticity is the local rotation of the primitive lattice in the moiré cell. We speculate that it is the local rotation, i.e., the vorticity of atomic displacements, rather than strain (the symmetric part of deformation tensor), that mostly controls the moiré potentials.

RESULTS

Figure 1A displays the optimized atomic structure of a $WSe_2/MoSe_2$ bilayer twisted by 2.65° from the H-type stacking. Zoomed in are the three local atomic configurations with 3-fold rotational symmetry, denoted as $H^{W,Se}_{Se,Mo}$, H^{W}_{Mo}, and H^{Se}_{Se}, respectively. Twisting modifies the electronic structure of a $WSe_2/MoSe_2$ bilayer and gives rise to moiré potentials. That is, the energy level of valence conduction bands will now vary with location in the moiré cell. With the knowledge that both the valence and conduction bands near the fermi level are contributed mainly by transition-metal ions in TMDC monolayers or bilayers, we have examined the local density of states (LDOSs) at the W and Mo atoms in the moiré cell. We have followed Carr et al.[10] in making use of the logarithm of LDOS to evaluate the VBM and CBM to make the displacement of LDOS curves more visible, as we did in our previous works.[21] We plot in Figure S1 the LDOS at 3-fold symmetry points $H^{W,Se}_{Se,Mo}$, H^{W}_{Mo}, and H^{Se}_{Se} in the moiré cell for θ_M = 2.65°. It is found that at each high-symmetry point, the VBM is mainly contributed by W in the WSe_2 layer and the CBM by Mo in the $MoSe_2$ layer. This is also demonstrated clearly in the species-projected band structure in Figure S2. The calculated energy levels of valence top and conduction bottom located at W and Mo atoms in the fully relaxed bilayer are shown in Figure 1B in the top and middle panels, respectively. In the bottom panel, we display their values along the diagonal of the moiré cell. The spatial variation of VBM and CBM defines the valence and conduction band moiré potentials. It is found that both of them reach a maximum at $H^{W,Se}_{Se,Mo}$ and a minimum at H^{W}_{Mo} with depths of 0.124 and 0.084 eV, comparable to the measured values, which were estimated to be about 0.2 and 0.1 eV.[12]

To illustrate the effect of lattice deformation on the band structure of single layers, we separated the fully relaxed bilayer into two isolated single layers and kept their atomic structure fixed. The calculated spatial distribution of the VBM at W atoms in the WSe_2 layer and CBM at Mo atoms in the $MoSe_2$ layer is shown in Figure 1C. Interestingly, we find that the lattice deformation induced by interlayer coupling in the moiré structure produces strong spatial variation of both VBM and CBM in single layers to an extent quite comparable to that in the bilayer. To further clarify the effect of lattice corrugation, we have performed a set of calculations for a flat $WSe_2/MoSe_2$ bilayer. That is, we have fixed the vertical positions of all the atoms and allowed only 2D relaxation. The interlayer distance was fixed at 6.74 Å, the average of the fully

[1]School of Materials Science and Engineering, Hainan University, Haikou 570228, China

[2]National Institute for Materials Science, Tsukuba 305-0044, Japan

[3]Department of Applied Physics, Xi'an University of Technology, Xi'an 710054, China

[4]Department of Physics, University of Science and Technology Beijing, Beijing 100083, China

[5]Institute of Mechanics, Chinese Academy of Sciences, Beijing 100190, China

[6]Lead contact

*Correspondence: geng@hainanu.edu.cn (W.T.G.), nara.jun@nims.go.jp (J.N.)

https://doi.org/10.1016/j.matt.2022.11.014

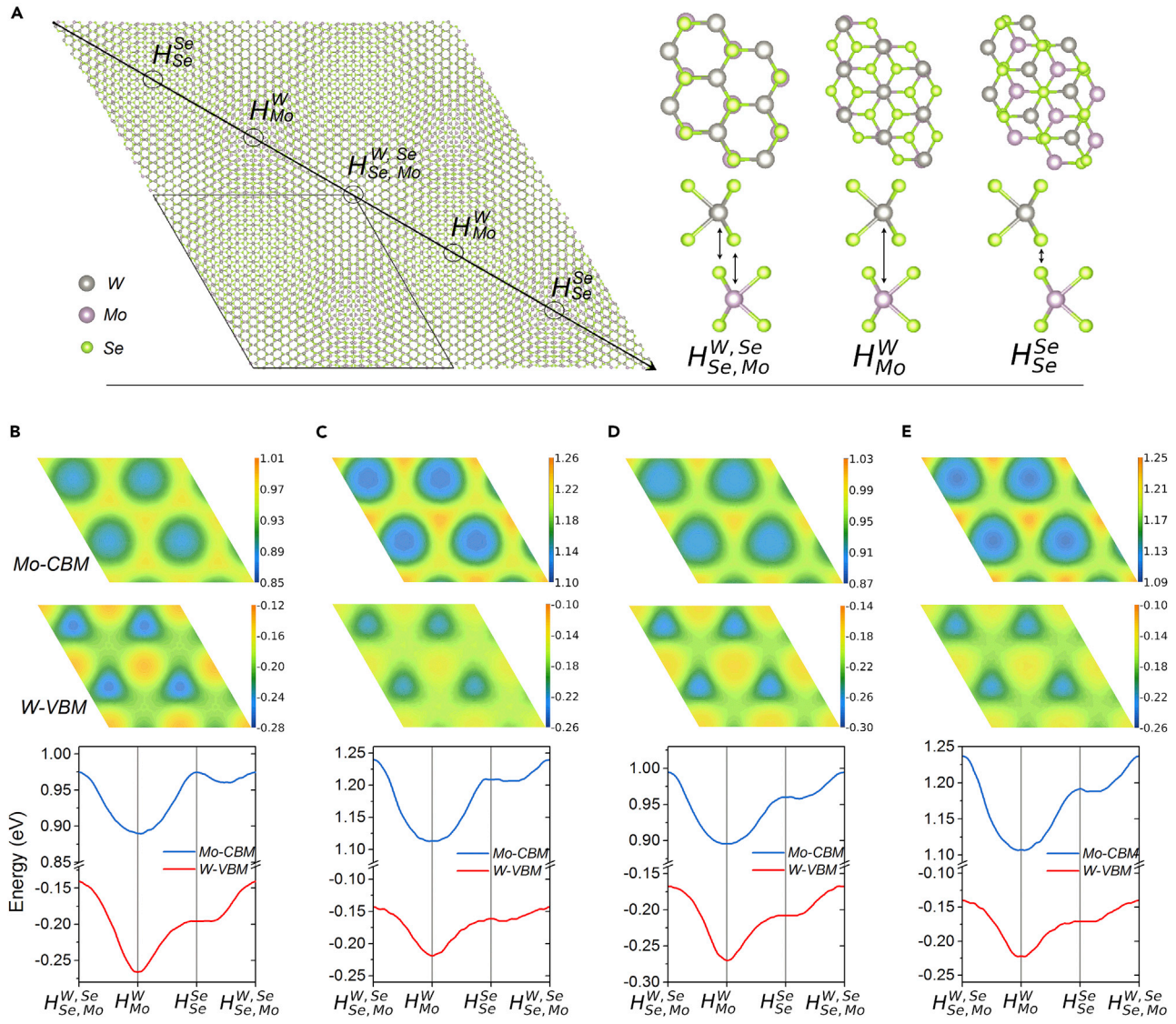

Figure 1. Moiré potentials in the 2.65° twisted H-stacking $WSe_2/MoSe_2$ bilayer

(A) The geometry of H-stacking $WSe_2/MoSe_2$ bilayer, and the high-symmetry points.

(B–E) Variations of conduction band minimum at Mo atoms (top) and valence band maximum at W atoms (middle) and their values along the diagonal in the moiré cell (bottom) of the fully relaxed, corrugated bilayer (B), isolated monolayers rigidly separated from the fully (3D) relaxed bilayer (C) and the 2D relaxed (flat) bilayer (D), and isolated monolayers rigidly separated from the 2D relaxed bilayer (E). The fermi level is set to zero.

relaxed bilayer. The results are displayed in Figure 1D. A comparison with Figure 1B shows that the lattice corrugation changes the shape remarkably rather than the depth of the moiré potentials. The impact is more significant on the $MoSe_2$ layer than the WSe_2 layer. In fact, the lattice corrugation raises the energy level of CBM at H^{Se}_{Se} almost up to the level at $H^{W,Se}_{Se,Mo}$, but its effect on WSe_2 is less significant. As for the fully relaxed bilayer, we also calculated the moiré potentials in the rigid single layers isolated from this 2D relaxed bilayer. Again, we find in Figure 1E that the lattice deformation has a strong influence on the electronic structure of the component single layers.

Figure 2A presents the calculated moiré potential depth of the valence (down triangles) and conduction (up triangles) bands for a $WSe_2/MoSe_2$ bilayer with a variety of

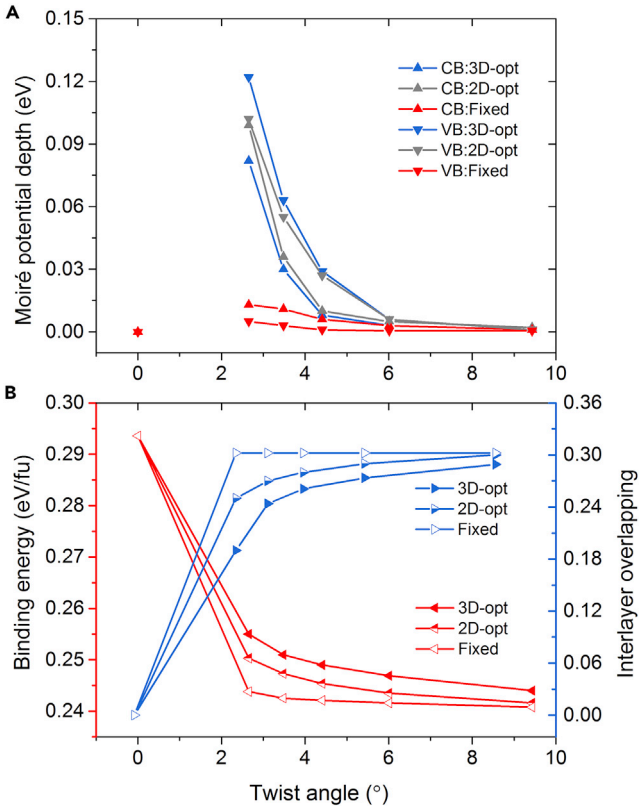

Figure 2. Twist-angle dependence of moiré potential

(A) Dependence of the valence and conduction bands moiré potential well depth in twisted WSe_2/$MoSe_2$ bilayer on the twist angle.

(B) Change of the interlayer binding strength and interlayer overlapping degree over the twist angle. Solid lines are a guide for the eye.

twist angles ($2.5° < \theta_M < 10°$), in rigid and 2D- and 3D-optimized configurations. Clearly, the moiré potentials (MPs) for both VB and CB in the rigid bilayers are negligibly small compared with those in the 2D and 3D relaxed structures. This is strong first-principles support for the conclusion drawn from continuum mechanical calculations[12] that, other than direct interlayer coupling, the internal strain dominates the MPs in twisted TMDC bilayers. For both VB and CB, the MP increases with the decreasing twist angle (increasing moiré wavelength). We note that limited by computational capacity, the smallest twist angle explored in the present study (2.65°) is not small enough ($\approx 1°$) for lattice reconstruction to take place, which leads to the formation of commensurate stacking domains separated by a network of domain walls bearing large strains.[22,23] Therefore, it is very interesting to discover that even without reconstruction, the local lattice-deformation-induced MP is bound to reach its maximum at a certain small twist angle before diminishing down to zero at $\theta_M = 0$.

To examine the effect of lattice deformation on the interlayer binding, we have calculated the interlayer binding energy of an H-stacking WSe_2/$MoSe_2$ bilayer as a function of the twist angle for fixed and 2D- and 3D-optimized configurations. The interlayer binding strength is defined as the lowering of the total free energy when two freestanding monolayers (WSe_2 and $MoSe_2$) are brought together to form a heterobilayer. The numerical results are displayed in Figure 2B (red

symbols). It turns out that without relaxation, the interlayer binding energy is nearly independent of the twist angle, strongly indicating that twisting has only marginal impact on the direct interlayer coupling. Upon relaxation, however, the binding strength reduces markedly with the increase of the twist angle, which can be understood by virtue of the concept of interlayer overlapping degree (IOD). IOD is a geometric quantity we recently proposed to describe the steric effect resulting from repulsive forces between overlapping electron clouds of the two contacting atomic layers across the interface.[21] These two layers in the present heterobilayer are the bottom Se layer in WSe_2 and the top Se layer in $MoSe_2$. In analog to graphene, we define the atomic radius of Se as $(\sqrt{3}/6)a$ of its respective primitive cell. Then, the IOD of the $WSe_2/MoSe_2$ heterobilayer can be calculated as the ratio of the total overlapping area of Se atoms across the interface to the total area covered by Se in the moiré cell. One Se atom covers $\sqrt{3}\pi/18$ of a primitive cell. The calculated IOD for both fixed and optimized heterobilayers with different twisting is displayed in Figure 2B (blue symbols). Clearly, the IOD increases with increasing twist angles, just opposite to the binding strength. Lattice deformation tends to decrease the IOD to reduce repulsive interactions but, in the meantime, suffers elastic energy cost. In the optimized geometry, an equilibrium is reached.

DISCUSSION

Having confirmed that it is the lattice deformation that yields the significant MP in twisted $WSe_2/MoSe_2$ bilayers, we now explore its effect in detail. In Figure 3, we present the deformation specifics of the twisted $WSe_2/MoSe_2$ bilayer with a twist angle of 2.65°. Figure 3A reveals the displacement of all W and Mo atoms upon geometry optimization in reference to those in the rigidly twisted bilayer. The displacement vectors are the 2D projection of the 3D ones.

Figure 3B shows the corrugation of the bilayer along the diagonal of the moiré cell. Points with 3-fold rotational symmetry are all at extrema of heights, and W and Mo are always corrugating in an opposite direction, as expected. Clearly, it takes the largest value at H_{Se}^{Se} (7.05 Å), the smallest at $H_{Se,Mo}^{W,Se}$ (6.52 Å), and a slightly higher local minimum at H_{Mo}^{W} (6.64 Å). In an analog-to-chemical bonding, the moiré effect of the vdW interactions at these high-symmetry points is in nonbonding, antibonding, and bonding states. Compared with that for twist-free stackings H_{Se}^{Se} (6.77 Å), $H_{Se,Mo}^{W,Se}$ (6.51 Å), and H_{Mo}^{W} (6.50 Å), the interlayer distance in a slightly twisted $WSe_2/MoSe_2$ bilayer is notably larger due to lattice deformation. Interestingly, we find that the difference at $H_{Se,Mo}^{W,Se}$ and H_{Mo}^{W}, which is responsible for the MPs, comes to be much more significant.

We learn from Figure 1 that the corrugation of the bilayer does not much affect the MP; this means that the 2D atomic displacements dominate the MP. The deformation tensor in a condensed matter system can be expressed as

$$D_{ij} = \frac{\partial u_i}{\partial x_j} = \frac{1}{2}\left(\frac{\partial u_i}{\partial x_j} + \frac{\partial u_j}{\partial x_i}\right) + \frac{1}{2}\left(\frac{\partial u_i}{\partial x_j} - \frac{\partial u_j}{\partial x_i}\right), \quad \text{(Equation 1)}$$

where $\vec{u} = \begin{pmatrix} u_i & u_j & u_k \end{pmatrix} = \vec{r} - \vec{r}_0$ is the displacement vector field before and after deformation at point $\vec{r}_m = \frac{1}{2}(\vec{r} - \vec{r}_0)$. The symmetric parts are the strain tensor, of which the diagonal terms

$$e_{ij} = \frac{1}{2}\left(\frac{\partial u_i}{\partial x_j} + \frac{\partial u_j}{\partial x_i}\right) \quad \text{(Equation 2)}$$

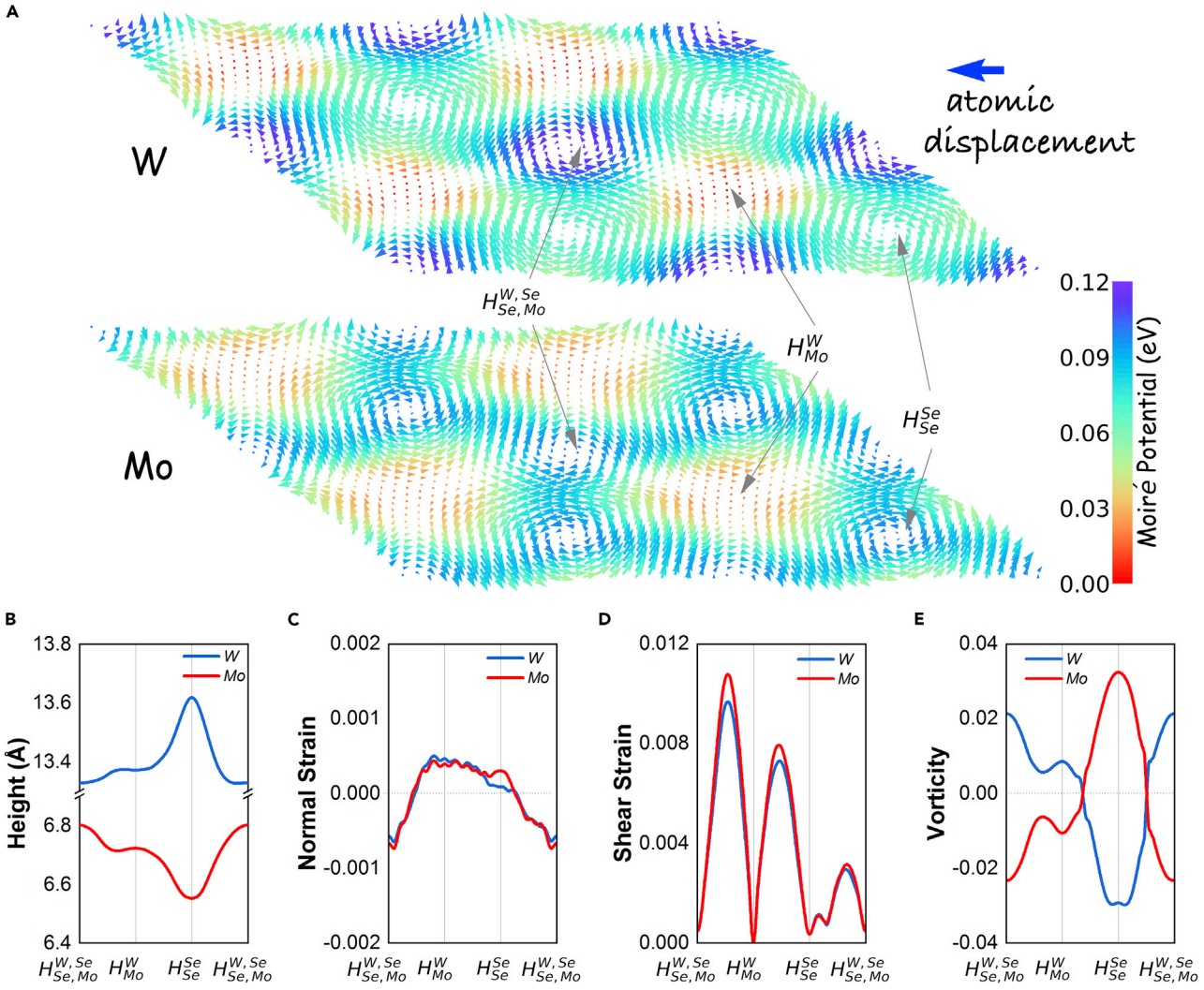

Figure 3. Lattice deformation

(A) Atomic displacements upon relaxation colored with moiré potential, represented by W and Mo atoms, of a $WSe_2/MoSe_2$ bilayer with a twist angle of 2.65°.

(B–E) Lattice corrugation (B), normal strain (C), magnitude of shear strain (D), and vorticity (in radian) of atomic displacements (E); numerical values along the diagonal of the moiré cell. Anticlockwise rotation in (E) is defined as being positive.

are the normal strain responsible for the rate of volume dilation and the off-diagonal parts are the shear strain, representing the change of shape of primitive atomic structure unit. The antisymmetric parts are the vorticity tensor,

$$\Omega_{ij} = \frac{1}{2}\left(\frac{\partial u_i}{\partial x_j} - \frac{\partial u_j}{\partial x_i}\right), \qquad \text{(Equation 3)}$$

which describes the rotation of the local atomic structure represented by primitive unit cells. Figures 3C–3E present the calculated normal strain, shear strain, and vorticity of the lattice deformation in WSe_2 and $MoSe_2$ layers, respectively. The normal strain is rather small in both layers, about −0.05%, and 0.05% at $H^{W,Se}_{Se,Mo}$ and H^{W}_{Mo}. Our first-principles calculations show that such strains will introduce a shift of −0.01 eV, 0.01 eV to the VBM, and 0.00 eV, −0.01 eV to the CBM, for twist-free $H^{W,Se}_{Se,Mo}$ and H^{W}_{Mo} -type stacking $WSe_2/MoSe_2$ heterobilayers (Figure S3). Thus, the spatial variation of VBM and

CBM is within 0.01 eV, an order smaller than the moiré well depths. Therefore, it is conclusive that normal strain has only a minor impact on the MPs at $\theta_M = 2.65^\circ$. The calculated shear strain shown in Figure 3D, like normal strain, is also in good agreement with the result of continuum mechanical calculations.[12]

We emphasize that the shear strain has vanishing value at the high-symmetry points where MPs reach their extrema. This strongly suggests that, other than normal strain and shear strain, there must be another quantity of the lattice deformation that is responsible for the generation of MPs. It is the vorticity of the atomic displacements that remind us to study the rotation, aside from the strain, in order to understand the origin of MPs. Vorticity serves as a descriptor of the rate of rotation of primitive unit cells in WSe_2 and $MoSe_2$ layers with respect to its original position in the rigidly twisted bilayer. The vorticity of lattice deformation displayed in Figure 3E, $\vec{\omega}$, is defined as

$$\vec{\omega} = \nabla \times \vec{u} = \left(\frac{\partial}{\partial x_i}, \frac{\partial}{\partial x_j}, \frac{\partial}{\partial x_k}\right) \times \left(u_i, u_j, u_k\right). \quad \text{(Equation 4)}$$

We can obtain a vorticity, which is the curl of the displacement of the atomic positions, as

$$\text{curl } \vec{u}\left(\vec{r}_a\right) \cdot \vec{n} = \lim_{\Delta S_n} \frac{1}{|\Delta S_n|} \oint_{P_n} \vec{u} \cdot d\vec{l}, \quad \text{(Equation 5)}$$

where P_n is the integration path with a surface $\vec{n}$, S_n is the area of the integration surface, and $d\vec{l}$ is the unit vector along the path. Here, in this case, the integration path is along the displacement vector field $\vec{u}$ of the nearest neighbors of six atoms, so the path integral can be expressed by a summation of the neighbor's contribution. For each neighbor, a sphere with radius $\left|\vec{r}_{nb}\right| = \left|\vec{r}_m - \vec{r}_a\right|$ is the integral path, so Equation 5 can be expressed as

$$\text{curl } \vec{u}\left(\vec{r}_a\right) \cdot \vec{n} = \sum_{nb}^{N} \frac{1}{|\Delta S_{nb}|} \frac{\left(\vec{r}_{nb} \times \vec{u}\right) \cdot \hat{n}}{\left|\vec{r}_{nb}\right|} \theta_{nb} \left|\vec{r}_{nb}\right| = \sum_{nb}^{N} \frac{1}{3\left|\vec{r}_{nb}\right|^2} \left(\vec{r}_{nb} \times \vec{u}\right) \cdot \hat{n}, \quad \text{(Equation 6)}$$

where $\Delta S_{nb} = \pi\left|\vec{r}_{nb}\right|^2$ and θ_{nb} is $\frac{\pi}{3}$, the radian contribution for each neighbor.

Interestingly, we find that the vorticity takes its local maximum and minimum at the high-symmetry points where MPs also reach their extrema. This is a strong indication that vorticity plays a dominant role in the generation of MPs. In addition, it is revealed that the distribution of vorticity has a pattern quite similar to that of the lattice corrugation. At H_{Se}^{Se}, the bilayer bulges the most, and the vorticity of atomic displacements is also the largest; at $H_{Se,Mo}^{W,Se}$ and H_{Mo}^{W}, the interlayer distance reaches the local minimum, as does the vorticity. Therefore, vorticity can serve as an ideal quantity to measure the moiré lattice deformation.

Having shown that it is the vorticity of lattice deformation at $H_{Se,Mo}^{W,Se}$ and H_{Mo}^{W} that dominates the MPs, we now investigate the dependence of ω on the twist angle of the $WSe_2/MoSe_2$ bilayer. Results for the W (up triangles) and Mo (down triangles) sublattices from first-principles calculations are demonstrated in Figure 4. We see that the vorticity of displacement of W and Mo at both $H_{Se,Mo}^{W,Se}$ (solid symbols) and

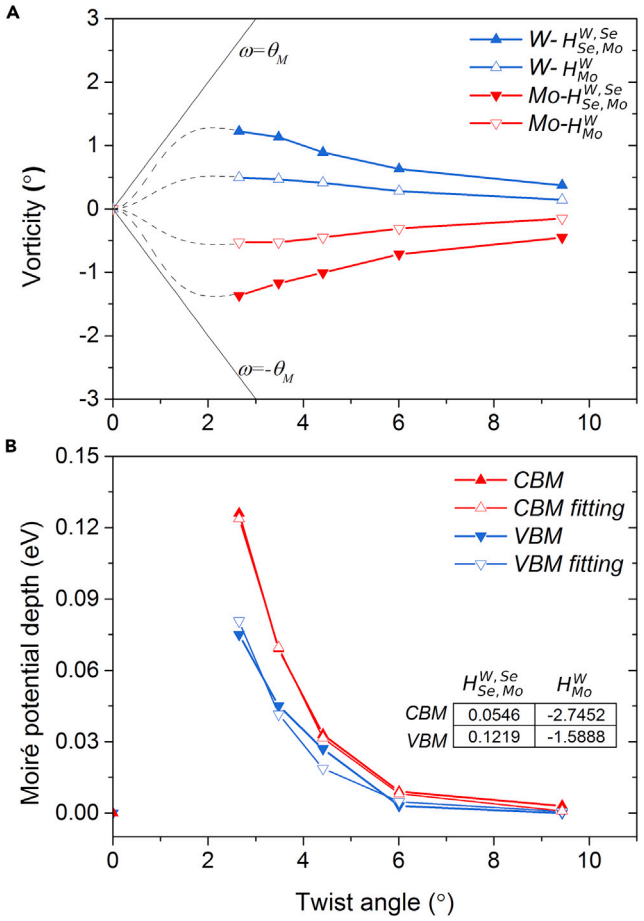

Figure 4. Vorticity of atomic displacement

(A) Vorticity of atomic displacements of W and Mo atoms at high-symmetry points in twisted $WSe_2/MoSe_2$ heterobilayers. Dashed lines are rough estimates of the vorticity variation at small twist angles.

(B) Comparison of the valence band (WSe_2) and conduction band ($MoSe_2$) moiré potential depth in monolayers rigidly separated from twisted $WSe_2/MoSe_2$ heterobilayers, obtained by first-principles calculations (solid symbols) and estimated from vorticity of atomic displacements upon structure relaxation (empty symbols).

H^W_{Mo} (empty symbols) increase monotonically with the decreasing twist angle, and their difference shows a similar feature. Our first-principles calculations thus strongly suggest that the vorticity of atomic displacements, rather than strain, of the lattice deformation plays dominant roles in the emergence of MPs for $2.5° < \theta_M < 10°$. As shown in Figure 4A, the vorticity of lattice deformation is zero in the twist-free $WSe_2/MoSe_2$ bilayer, that is, if $\theta_M = 0$, then $\omega = 0$. There must exist a critical twist angle at which the vorticity takes its maximum value, which probably falls in the region 1°–2°, as MPs do, before lattice reconstruction occurs. It is noteworthy that ω, by definition, is two times as large as the rotation angle of the hexagon centered at the W or Mo atom of concern. Since the local lattice rotation in one monolayer is a kind of resistance to the increase of the IOD (steric effect) induced by the global rotation θ_M in reference to the other monolayer, we should have $\omega \leq \theta_M$. As for the flat, 2D-optimized bilayer, similar results are obtained (Figure S4). Although the maximum vorticity (at H^{Se}_{Se}) in the 2D-optimized $WSe_2/MoSe_2$ bilayer is even slightly higher than in the corrugated, 3D-optimized case, the vorticity difference at $H^{W,Se}_{Se,Mo}$

and H_{Mo}^{W} is a bit smaller than in the latter geometry. The reason 2D and 3D optimization yield vorticity of lattice deformation in a similar scale is that in the restricted 2D deformation, the tendency of the bilayer to corrugate is suppressed and compensated for by enhanced planar atomic displacements.

Keeping in mind that the MP is induced by nonuniform interlayer coupling and that it varies in the moiré cell in a similar manner to the vorticity of atomic displacements, we attempt to correlate the moiré well depth with the difference of vorticity at high-symmetry points $H_{Se,Mo}^{W,Se}$ and H_{Mo}^{W} and make a connection between the band energy of electrons and elastic energy density in the local lattice of distorted WSe_2 and $MoSe_2$ monolayers. This idea is inspired by previous study investigating the relationship between strain and band gap on a strained vdW black phosphorus monolayer.[24] We assume that the band energy E at a lattice point depends on the elastic energy per unit area at this point, E_e , in the form of

$$E = E_0 + \Gamma \cdot E_e, \qquad \text{(Equation 7)}$$

where E_0 is the band energy in a distortion-free monolayer and Γ is the local enhancement coefficient, which is band dependent. E_0 does not change over the moiré cell, thus the difference in the electric potential at two lattice points (α, β) can be written as

$$\Delta E(\alpha, \beta) = \Gamma_\alpha \cdot E_e(\alpha) - \Gamma_\beta \cdot E_e(\beta), \qquad \text{(Equation 8)}$$

in which α and β stand for antibonding $H_{Se,Mo}^{W,Se}$ and bonding H_{Mo}^{W} lattice points, respectively. At the high-symmetry lattice points, i.e., the centers of the vortices of atomic displacements, both normal and shear strains are negligibly small (Figures 3C and 3D). It is found that the elastic energy has the following relationship between the vorticity (ω) and the twisted angle (θ_M):

$$E_e = \frac{1}{2}\kappa\omega^2 \propto a_M^2\omega^2 \propto (\omega/\theta_M)^2 . \qquad \text{(Equation 9)}$$

Here, the elastic coefficient κ is material dependent and assumed to be proportional to the area of the vortex of atomic displacements $\left(\frac{\sqrt{3}}{6}a_M^2\right)$. Therefore, the difference in band energy between the two vortex centers can be estimated as

$$\Delta E(\alpha, \beta) \cong C_\alpha \cdot (\omega_\alpha/\theta_M)^2 - C_\beta \cdot (\omega_\beta/\theta_M)^2, \qquad \text{(Equation 10)}$$

where C_α and C_β are functions of both Γ and κ and hence are all band- and material-dependent coefficients. For both VB and CB, which are contributed mainly by cations, the value of C is found to be large in the vortex centered at Mo or W (H_{Mo}^{W}), rather small in those centered at the hollow sites ($H_{Se,Mo}^{W,Se}$), and even smaller in those at the anions (H_{Se}^{Se}) (see Figure S5). In Figure 4B, the fitting of MPs for both VB in WSe_2 and CB in $MoSe_2$ monolayers from vorticity of atomic displacements (empty symbols) agrees well with the results of first-principles calculations (solid symbols).

According to fluid dynamics, the vortices in a 2D system have a tendency to merge and form larger vortices, and those in a 3D system are prone to be torn apart into smaller ones by the vertical motions to release kinetic energies.[20] Although vdW bilayers are not strictly 2D, as they have the freedom to corrugate, the strong in-plane chemical bonds hold the corrugation slope to be rather limited, and the z component of the vorticity vector is predominant over x and y components. Thus, it is reasonable to expect that the vortices of atomistic displacements are inclined to

coalesce to reduce elastic energies, which leads to the reconstruction of the moiré cell at very small twist angles.[22,23]

The formation of commensurate stacking domains separated by a network of domain walls in a twisted TMDC bilayer upon lattice reconstruction results in the concentration and enhancement of lattice strains at domain walls, and large normal strains bring about significant MPs. In a newly reported computational work, Enaldiev et al. applied a multiscale modeling approach[23] to study the effect of normal strain on the shift of valence and conduction band edges and electron/hole confinement in such domains using density functional theory (DFT) parametrized interpolation formulae for interlayer adhesion energies of TMDC monolayers and the elasticity theory for strain-related elastic energies. Excitingly, they found that the normal strain in a marginally twisted $WSe_2/MoSe_2$ heterobilayer can be as large as 0.06 and that the MPs can reach 1 eV.[25] Such strong MPs could lead to significant red shift of the electron-hole recombination line, making single photon emitters broadly tunable and hence enabling the manipulation of nanoscale commensurate domains in moiré patterns as effective quantum dots.

For $\theta_M = 1.0°$, Enaldiev et al. predicted a moiré depth of 0.1 eV for the VBM and 0.2 eV for the CBM. The experimental results in Shabani et al.[12] are about 0.3 and 0.15 eV, respectively. At $\theta_M = 1.5°$, Shabani et al.[12] found a maximum of MPs for both VBM and CBM; Enaldiev et al.,[25] on the other hand, did not reproduce this phenomenon. For $\theta_M = 2.65°$, our first-principles DFT calculations give a band-gap modulation of 0.06 eV, significantly smaller than the estimation in Enaldiev et al.,[25] which is about 0.3 eV; as for the magnitude of normal strain, our prediction is about 0.0005, 10 times smaller than the result in Enaldiev et al.[25] Therefore, it appears that the multiscale modeling approach used by Enaldiev et al. to evaluate the lattice strain may not be as accurate for $\theta_M \geq 1.0°$ as for marginally small angles ($0° < \theta_M < 1°$), which correspond to huge moiré supercells and justify ideally the application of elasticity theory in continuum mechanics. The effect of the vorticity of atomic displacements on the shift of band edges, which is predicted to be significant for ($1° < \theta_M < 4°$) in the present work, has not been explored in Enaldiev et al.[25]

For TMDC bilayers that have large lattice mismatch, such as MoS_2/WSe_2 and WS_2/WSe_2,[26,27] moiré patterns can be formed at a zero twist angle. The vorticity of atomic displacements in these systems is expected to be negligible, so the origin of MPs from lattice deformation is predominantly the normal strain. To make a comparison of normal strain and vorticity about their efficiency in generating MPs, we have performed DFT calculations on the structural and electronic properties of twist-free $MoS_2/MoSe_2$ and $MoSe_2/MoTe_2$ bilayers. The supercells used to model these two systems are $MoS_2(24 \times 24)/MoSe_2(23 \times 23)$ and $MoSe_2(15 \times 15)/MoTe_2(14 \times 14)$, respectively. The former moiré cell, which contains 3,315 atoms, is displayed in Figure S6A together with its high-symmetry local structures AA, AB, and BA.

Different from the twisted $WSe_2/MoSe_2$ bilayer case, the VBM and CBM MPs in these twist-free bilayers vary in antiphase (Figures S6B–S6E). That is, when the VBM shifts up, the CBM shifts down (and vice versa). This is because the direction of the local lattice rotation vector in one layer is always opposite to that in the other layer and has no absolute meaning, but positive and negative strains (Figure S7) represent opposite lattice dilation (enlargement and reduction), respectively. Interestingly, we find the MPs in the twist-free $MoS_2(24 \times 24)/MoSe_2(23 \times 23)$ bilayer have similar strength (~0.1 eV) to those in the twisted $WSe_2/MoSe_2$ bilayer at $\theta_M = 2.65°$. For the $MoSe_2$ layer, the maximum normal strain in the former bilayer is about 0.006,

Table 1. Size dependence of twist angle to the model H-stacking $WSe_2/MoSe_2$ heterobilayers

θ_M (°)	2.65°	3.48°	4.41°	6.01°	9.43°
N_{atom}	2,814	1,626	1,014	546	222
a_M (Å)	71.27	54.18	42.78	31.39	20.02

The moiré wavelength a_M, twist angle θ_M, and total number of atoms N_{atom} used in the supercells.

whereas the vorticity in the latter is about 0.03, seemingly indicating that normal strain is more efficient in prompting MPs. Nevertheless, a slightly weaker normal-strain field in the $MoSe_2$ layer in the twist-free $MoSe_2(15 \times 15)/MoTe_2(14 \times 14)$ bilayer gives rise to much smaller MP (~0.01 eV). Such a disparity is probably originated from the dissimilarity of the two bilayers in interlayer charge transfer. We note that the electronegativities of S (2.58) and Se (2.55) are quite similar, but it is weaker for Te (2.10). A more detailed analysis of the twist-free case and a more general model to consider normal strain and vorticity altogether are desirable but are beyond the scope of the present work.

Our first-principles DFT calculations on twisted $WSe_2/MoSe_2$ heterobilayers reveal that the MPs of both valence and conduction bands increase with decreasing twist angle, reaching values significantly larger than that of unstrained twist-free bilayers. Comparison between fixed and fully relaxed configurations demonstrates that the direct interlayer binding has only a marginal effect on the MP and that the lattice deformation plays a dominant role. The normal strain is too small to have strong impact to the MP. The shear strain, on the other hand, is not correlated directly to the MP. Our striking discovery is that the vorticity of atomic displacements, i.e., the rotation of primitive unit cells in the moiré cell, dominates the MPs. This finding could open up new avenues in band-structure engineering of vdW heterostructures via lattice deformation. Description of atomistic displacement vectors in framework of fluid dynamics might be fruitful in exploring novel phenomena in twistronics.

EXPERIMENTAL PROCEDURES

Resource availability

Lead contact

Further information and requests for resources should be directed to and will be fulfilled by the lead contact, Wen Tong Geng (geng@hainanu.edu.cn).

Materials availability

This study was purely computational and did not generate new unique reagents.

Data and code availability

All data are available in the main text or the supplemental information.

Computational methods

We have investigated five twist angles starting from the H-type (antiparallel) $WSe_2/MoSe_2$ bilayer. The total number of atoms and the 2D length (moiré wavelength) of these supercells are listed in Table 1. In each moiré cell, the length in the c axis was set to 30 Å. The vacuum region in such a supercell is about 20 Å, large enough to minimize the bilayer-bilayer interactions between neighboring supercells. The lattice mismatch of WSe_2 (3.303 Å) and $MoSe_2$ (3.297 Å) is very small (0.2%) and is neglected in this study. Since the interlayer charge transfer is extremely small (2.2×10^{-4} e per formula unit $WSe_2/MoSe_2$), there is no need to double the supercell size and include both a $MoSe_2/WSe_2$ and a $WSe_2/MoSe_2$ bilayer as is the case for $MoTe_2/MoS_2$ heterobilayers.[13]

The DFT calculations were performed using the Vienna Ab initio Simulation Package.[28] We described the electron-ion interactions with the projector augmented-wave (PAW) method,[29] the exchange correlation between electrons within the generalized gradient approximation (GGA) in the Perdew-Burke-Ernzerhof (PBE) form,[30] and the nonbonding vdW interactions using a semi-empirical correction scheme of the DFT-D3 method.[31] An energy cutoff of 400 eV was employed for the plane-wave basis set for all systems to ensure. We made the Brillouin-zone integration within the Monkhorst-Pack scheme[32] using k meshes of (1 × 1 × 1) for twist angles 2.65° and 3.48°, (2 × 2 × 1) for 4.41° and 6.01°, and (3 × 3 × 1) for 9.43°. The dimensions of the supercell were fixed, and the internal freedoms of all atoms were fully optimized. In structural optimization, the self-consistency criterion for the total energy of the supercell and forces on all the atoms were set to be 10^{-4} eV/cell and 2×10^{-2} eV Å^{-1}, respectively. To make the computation affordable, we did not take into account spin-orbit coupling. In generating the initial atomic structure and plotting the band structure of supercells, we have used the VASPKIT code.[33]

SUPPLEMENTAL INFORMATION

Supplemental information can be found online at https://doi.org/10.1016/j.matt.2022.11.014.

ACKNOWLEDGMENTS

The calculations were performed on the Numerical Materials Simulator of NIMS. This work was funded by the Innovative Science and Technology Initiative for Security, ATLA, Japan (no. JPJ004596) (W.T.G., T.O., and J.N.); the National Natural Science Foundation of China (no. 62174136) (V.W.); and the LiYing Program of the Institute of Mechanics, Chinese Academy of Sciences (no. E1Z1011001) (Q.P.)

AUTHOR CONTRIBUTIONS

Conceptualization, W.T.G.; methodology, W.T.G., J.B.L., and J.N.; investigation, W.T.G., J.B.L., V.W., Q.G., Q.P., T.O., and J.N.; visualization, W.T.G. and J.B.L.; funding acquisition, T.O., J.N., and V.W.; project administration, T.O. and J.N.; supervision, W.T.G., Q.G., Q.P., T.O., and J.N.; writing – original draft, W.T.G., J.B.L., T.O., and J.N.; writing – review & editing, W.T.G., J.B.L., V.W., Q.G., Q.P., T.O., and J.N.

DECLARATION OF INTERESTS

The authors declare no competing interests.

Received: July 8, 2022
Revised: September 1, 2022
Accepted: November 10, 2022
Published: December 5, 2022

REFERENCES

1. Dean, C.R., Wang, L., Maher, P., Forsythe, C., Ghahari, F., Gao, Y., Katoch, J., Ishigami, M., Moon, P., Koshino, M., et al. (2013). Hofstadter's butterfly and the fractal quantum Hall effect in moiré superlattices. Nature *497*, 598–602. https://doi.org/10.1038/nature12186.

2. Hunt, B., Sanchez-Yamagishi, J.D., Young, A.F., Yankowitz, M., LeRoy, B.J., Watanabe, K., Taniguchi, T., Moon, P., Koshino, M., Jarillo-Herrero, P., and Ashoori, R.C. (2013). Massive Dirac fermions and hofstadter butterfly in a van der Waals heterostructure. Science *340*, 1427–1430. https://doi.org/10.1594/PANGAEA.808834.

3. Tran, K., Moody, G., Wu, F., Lu, X., Choi, J., Kim, K., Rai, A., Sanchez, D.A., Quan, J., Singh, A., et al. (2019). Evidence for moiré excitons in van der Waals heterostructures. Nature *567*, 71–75. https://doi.org/10.1038/s41586-019-0975-z.

4. Alexeev, E.M., Ruiz-Tijerina, D.A., Danovich, M., Hamer, M.J., Terry, D.J., Nayak, P.K., Ahn, S., Pak, S., Lee, J., Sohn, J.I., et al. (2019). Resonantly hybridized excitons in moiré superlattices in van der Waals heterostructures. Nature *567*, 81–86. https://doi.org/10.1038/s41586-019-0986-9.

5. Seyler, K.L., Rivera, P., Yu, H., Wilson, N.P., Ray, E.L., Mandrus, D.G., Yan, J., Yao, W., and Xu, X. (2019). Signatures of moiré-trapped valley

excitons in MoSe2/WSe2 heterobilayers. Nature *567*, 66–70. https://doi.org/10.1038/s41586-019-0957-1.

6. Jin, C., Regan, E.C., Yan, A., Iqbal Bakti Utama, M., Wang, D., Zhao, S., Qin, Y., Yang, S., Zheng, Z., Shi, S., et al. (2019). Observation of moiré excitons in WSe2/WS2 heterostructure superlattices. Nature *567*, 76–80. https://doi.org/10.1038/s41586-019-0976-y.

7. Regan, E.C., Wang, D., Jin, C., Bakti Utama, M.I., Gao, B., Wei, X., Zhao, S., Zhao, W., Zhang, Z., Yumigeta, K., et al. (2020). Mott and generalized Wigner crystal states in WSe2/WS2 moiré superlattices. Nature *579*, 359–363. https://doi.org/10.1038/s41586-020-2092-4.

8. Tang, Y., Li, L., Li, T., Xu, Y., Liu, S., Barmak, K., Watanabe, K., Taniguchi, T., MacDonald, A.H., Shan, J., and Mak, K.F. (2020). Simulation of Hubbard model physics in WSe2/WS2 moiré superlattices. Nature *579*, 353–358. https://doi.org/10.1038/s41586-020-2085-3.

9. Liu, E., Barré, E., van Baren, J., Wilson, M., Taniguchi, T., Watanabe, K., Cui, Y.T., Gabor, N.M., Heinz, T.F., Chang, Y.C., and Lui, C.H. (2021). Signatures of moiré trions in WSe2/MoSe2 heterobilayers. Nature *594*, 46–50. https://doi.org/10.1038/s41586-021-03541-z.

10. Carr, S., Massatt, D., Fang, S., Cazeaux, P., Luskin, M., and Kaxiras, E. (2017). Twistronics: manipulating the electronic properties of two-dimensional layered structures through their twist angle. Phys. Rev. B *95*, 075420–075426. https://doi.org/10.1103/PhysRevB.95.075420.

11. Bistritzer, R., and MacDonald, A.H. (2011). Moiré bands in twisted double-layer graphene. Proc. Natl. Acad. Sci. USA *108*, 12233–12237. https://doi.org/10.1073/pnas.1108174108.

12. Shabani, S., Halbertal, D., Wu, W., Chen, M., Liu, S., Hone, J., Yao, W., Basov, D.N., Zhu, X., and Pasupathy, A.N. (2021). Deep moiré potentials in twisted transition metal dichalcogenide bilayers. Nat. Phys. *17*, 720–725. https://doi.org/10.1038/s41567-021-01174-7.

13. Geng, W.T., Wang, V., Liu, Y.C., Ohno, T., and Nara, J. (2020). Moiré potential, lattice corrugation, and band gap spatial variation in a twist-free MoTe2/MoS2 heterobilayer. J. Phys. Chem. Lett. *11*, 2637–2646. https://doi.org/10.1021/acs.jpclett.0c00605.

14. Yu, H., Liu, G.B., Tang, J., Xu, X., and Yao, W. (2017). Moiré excitons: from programmable quantum emitter arrays to spin-orbit–coupled artificial lattices. Sci. Adv. *3*, e1701696–e1701698. https://doi.org/10.1126/sciadv.1701696.

15. Conley, H.J., Wang, B., Ziegler, J.I., Haglund, R.F., Pantelides, S.T., and Bolotin, K.I. (2013). Bandgap engineering of strained monolayer and bilayer MoS2. Nano Lett. *13*, 3626–3630. https://doi.org/10.1021/nl4014748.

16. Dhakal, K.P., Roy, S., Jang, H., Chen, X., Yun, W.S., Kim, H., Lee, J., Kim, J., and Ahn, J.H. (2017). Local strain induced band gap modulation and photoluminescence enhancement of multilayer transition metal dichalcogenides. Chem. Mater. *29*, 5124–5133. https://doi.org/10.1021/acs.chemmater.7b00453.

17. Zollner, K., Junior, P.E.F., and Fabian, J. (2019). Strain-tunable orbital, spin-orbit, and optical properties of monolayer transition-metal dichalcogenides. Phys. Rev. B *100*, 195126. https://doi.org/10.1103/PhysRevB.100.195126.

18. Nelson, D.R., Piran, T., and Weinberg, S. (2004). Statistical Mechanics of Membranes and Surfaces (World Scientific).

19. Meyer, J.C., Geim, A.K., Katsnelson, M.I., Novoselov, K.S., Booth, T.J., and Roth, S. (2007). The structure of suspended graphene sheets. Nature *446*, 60–63. https://doi.org/10.1038/nature05545.

20. Currie, I.G. (2003). Fundamental Mechanics of Fluids (Marcel Dekker, Inc.).

21. Geng, W.T., Wang, V., Lin, J.B., Ohno, T., and Nara, J. (2021). Angle dependence of interlayer coupling in twisted transition metal dichalcogenide heterobilayers. J. Phys. Chem. C *125*, 1048–1053. https://doi.org/10.1021/acs.jpcc.0c09372.

22. Rosenberger, M.R., Chuang, H.J., Phillips, M., Oleshko, V.P., McCreary, K.M., Sivaram, S.V., Hellberg, C.S., and Jonker, B.T. (2020). Twist angle-dependent atomic reconstruction and moiré patterns in transition metal dichalcogenide heterostructures. ACS Nano *14*, 4550–4558. https://doi.org/10.1021/acsnano.0c00088.

23. Enaldiev, V.V., Zólyomi, V., Yelgel, C., Magorrian, S.J., and Fal'ko, V.I. (2020). Stacking domains and dislocation networks in marginally twisted bilayers of transition metal dichalcogenides. Phys. Rev. Lett. *124*, 206101. https://doi.org/10.1103/PhysRevLett.124.206101.

24. Rodin, A.S., Carvalho, A., and Castro Neto, A.H. (2014). Strain-induced gap modification in black phosphorus. Phys. Rev. Lett. *112*, 176801–176805. https://doi.org/10.1103/PhysRevLett.112.176801.

25. Enaldiev, V.V., Ferreira, F., McHugh, J.G., and Fal'ko, V.I. (2022). Self-organised quantum dots in marginally twisted MoS2/WSe2 and MoS/WS2 bilayers. Preprint at arXiv. https://doi.org/10.48550/ARXIV.2204.06823.

26. Zhang, C., Chuu, C.-P., Ren, X., Li, M.-Y., Li, L.-J., Jin, C., Chou, M.-Y., and Shih, C.-K. (2017). Interlayer couplings, Moiré patterns, and 2D electronic superlattices in MoS2/WSe2 heterobilayers. Sci. Adv. *3*, e1601459. https://doi.org/10.1126/sciadv.1601459.

27. Yuan, L., Zheng, B., Kunstmann, J., Brumme, T., Kuc, A.B., Ma, C., Deng, S., Blach, D., Pan, A., and Huang, L. (2020). Twist-angle-dependent interlayer exciton diffusion in WS2–WSe2 heterobilayers. Nat. Mater. *19*, 617–623. https://doi.org/10.1038/s41563-020-0670-3.

28. Kresse, G., and Furthmüller, J. (1996). Efficient iterative schemes for ab initio total-energy calculations using a plane-wave basis set. Phys. Rev. B Condens. Matter *54*, 11169–11186. https://doi.org/10.1103/PhysRevB.54.11169.

29. Blöchl, P.E. (1994). Projector augmented-wave method. Phys. Rev. B Condens. Matter *50*, 17953–17979. https://doi.org/10.1103/PhysRevB.50.17953.

30. Perdew, J.P., Burke, K., and Ernzerhof, M. (1996). Generalized gradient approximation made simple. Phys. Rev. Lett. *77*, 3865–3868. https://doi.org/10.1103/PhysRevLett.77.3865.

31. Klime, J., Bowler, D.R., and Michaelides, A. (2011). Van der Waals density functionals applied to solids. Phys. Rev. B *83*, 195131. https://doi.org/10.1103/PhysRevB.83.195131.

32. Pack, J.D., and Monkhorst, H.J. (1977). "Special points for Brillouin-zone integrations"-a reply. Phys. Rev. B *16*, 1748–1749. https://doi.org/10.1103/PhysRevB.16.1748.

33. Wang, V., Xu, N., Liu, J.C., Tang, G., and Geng, W.T. (2021). VASPKIT: a user-friendly interface facilitating high-throughput computing and analysis using VASP code. Comput. Phys. Commun. *267*, 108033. https://doi.org/10.1016/j.cpc.2021.108033.